Depósito de Investigación de la Universidad de Sevilla

https://idus.us.es/

Analytical expressions to estimate the effective piezoelectric tensor of a textured polycrystal for any crystal symmetry

Julieta L. Buroni

Facultad de Ciencias Exactas y Naturales, Universidad Nacional de Mar del Plata, Deán Funes 3350, B7602AYL, Mar del Plata, Argentina

Federico C. Buroni

E-mail: `fburoni@us.es`
Department of Mechanical Engineering and Manufacturing, Universidad de Sevilla, Camino de los Descubrimientos s/n, 41092, Seville, Spain

Adrián P. Cisilino

INTEMA & Department of Mechanical Engineering, Universidad Nacional de Mar del Plata & CONICET, Av. Juan B. Justo 4302, B7608FDQ Mar del Plata, Argentina

Roderick Melnik

MS2 Discovery Interdisciplinary Research Institute, Wilfrid Laurier University, 75 University Ave W, Waterloo, Ontario, Canada N2L 3C5

Luis Rodríquez-Tembleque and Andrés Sáez

Department of Continuum Mechanics and Structural Analysis, Universidad de Sevilla, Camino de los Descubrimientos s/n, Seville E-41092, Spain

Abstract. This work introduces a set of analytical expressions that simplifies the procedure of obtaining closed-form formulas to estimate the effective piezoelectric properties of polycrystalline aggregates formed by crystals of all the 21 non-centrosymmetrical classes and with arbitrary textures. The expressions are derived from orientational averages of third-order piezoelectric tensors of the individual crystals that are weighted by orientational distribution functions. The averaging is done by using generalized spherical harmonic series expansions. Improvements with respect to previous works in the literature are twofold: all crystal symmetries are considered and no symmetry restrictions are imposed to texture. The versatility of the introduced expressions is demonstrated on an example of $BaTiO_3$ polycrystals with uniaxial and biaxial textures characterized by single and double Gaussian distributions, respectively. The results for uniaxial texture are in perfect agreement with the results published in the literature. The biaxial texture is discussed in detail and analyzed for a set of limiting cases.

1. Introduction

Piezoelectric ceramics (Uchino, 2017) are generally used in the form of a collection of perfectly bonded piezoelectric crystals with a large number of distinct polarization orientations. Macroscopic piezoelectric properties of the material are governed by this microscopic inhomogeneous crystal morphology. When the material is an aggregate of randomly oriented piezoelectric crystals, no net polarization is realized and so the material is not macroscopically piezoelectric. To achieve macroscopic piezoelectric properties, the individual crystals must have a preferential orientation. Generally, piezoelectric properties exhibit large anisotropy, which is an attractive feature for material design. Preferred orientation of the crystallographic domains can be accomplished by controlling growth parameters during fabrication (Kim et al., 2006) or by subjecting the material to a large electric field at high temperature (Li et al., 2005).

Optimization methods can be used to design materials specific piezoelectric properties by tailoring their orientation distribution (texture). In the framework of the implementation of an optimization algorithm, Finite Element Analysis (FEA) is a versatile tool to compute effective piezoelectric properties (the optimization objective function) by means of a numerical homogenization approach, see for instance Jayachandran et al. (2011). However, closed-form analytical expressions for effective piezoelectric properties are always preferable over the FEA homogenization approach, as they simplify implementations and speed up calculations.

Effective piezoelectric properties can be estimated by averaging the properties of single crystals in the aggregate taking into account macroscopic texture. To calculate the effective properties for a polycrystal, the best averaging method is the self-consistent, extended to piezoelectric polycrystals by Li (2000). However this method requires computation of piezoelectric Eshelby tensor which involves, in general, numerical integration. On the other hand, there are the simple volume averaging approaches, like the Voigt model (see Li and Dunn (2001)), which are attractive because they allow to deduce closed-form expressions for the effective properties. In particular, the Voigt model assumes uniform strain and electric fields in the crystallites. This assumption is valid for piezoelectric polycrystals with fiber textures under certain conditions (see Li et al. (1999)) for which exact estimates of some of the electroelastic moduli result. Working in the context of fiber texture, Li et al. (1999) and Li (2000) computed Voigt-Reuss estimations for the electroelastic moduli of polycrystals by approaching the problem with generalized spherical harmonics. Specifically, Li et al. (1999) considered fiber texture of orthorhombic single crystals belonging to class symmetry *2mm*, which includes as particular cases classes of tetragonal *4mm* and hexagonal *6mm* symmetries (see Nye's book (Nye, 1985)). An interesting finding by Li (2000) was that aggregates of *4mm* crystals of barium titanate (BaTiO$_3$) with their orientations around the polarization direction characterized by a Gaussian distribution present an amplification effect of the piezoelectric coupling with respect to the single crystal properties. Recently, some of the

authors of the present work have used the Li's framework for modelling modern lead-free piezocomposites to find interesting behaviours attributable to such amplification effect of the polycrystalline phase (Krishnaswamy et al., 2019a,b, 2020a,b,c).

Previous works address only orthorhombic crystal symmetry with transversely isotropic texture. This work presents a comprehensive approach to derive closed-form expressions for the estimation of the effective piezoelectric stress tensor of crystal aggregates of any symmetry and general texture. The proposed approach is based on the previous works by Li et al. in the use of generalized spherical harmonics expansion and extends the ideas by Bunge (1982) and Roe (1965) among others, from elasticity to piezoelectricity.

The derived analytical expressions are verified and their versatility demonstrated through a study problem consisting in a polycrystalline aggregate of $BaTiO_3$ with various orientational distribution functions. It is shown how the general expressions introduced in this work can be reduced to those results by Li (2000) for specific cases.

The repeated index convention for addition is used in this work. Explicit sums are indicated in expressions when deemed convenient for the sake of clarity.

2. Preliminaries

We concern with the computation of the anisotropic electromechanical coupling of polycrystal piezoceramics from the properties of single crystallites and their orientations. A simple approximation to compute this coupling is through the volume average of the third-order piezoelectric stress tensor e_{ijk}, which satisfies $e_{ijk} = e_{ikj}$ $(i, j, k = 1 \ldots 3)$. Since in this case e_{ijk} depends only on the crystal orientation $g(x_i)$ $(i = 1 \ldots 3)$ at each point $\boldsymbol{x}$, the integration over a representative volume element V can be carried out in two steps, as usual. We first integrate over all those volume elements $\mathrm{d}V$ with orientation g, and then over all orientations g, thereby the average tensor is computed by

$$\langle \mathbf{e} \rangle = 8\pi^2 \oint \mathbf{e}(g)w(g)\mathrm{d}g, \tag{1}$$

where the function $w : SO(3) \to \mathbb{R}_{\geq 0}$ –called Orientation Distribution Function (ODF)– appears as a weight function that accounts for the volumetric density of crystallites oriented in $\mathrm{d}g$. This Haar measure $\mathrm{d}g$ is —after normalization— given by $\mathrm{d}g = 1/(8\pi^2) \sin\theta \mathrm{d}\theta \mathrm{d}\psi \mathrm{d}\phi$ where (ψ, θ, ϕ) are the Euler's angles. Then, the ODF is normalized such as

$$8\pi^2 \oint w(g)\mathrm{d}g = 1. \tag{2}$$

Therefore, by expressing the crystal orientation in terms of $(\psi, \xi = \cos\theta, \phi)$, the Voigt average becomes

$$\langle \mathbf{e} \rangle = \int_0^{2\pi} \int_0^{2\pi} \int_{-1}^{+1} \mathbf{e}(\xi, \psi, \phi)w(\xi, \psi, \phi)d\xi d\psi d\phi, \tag{3}$$

Note that the normalization factor $8\pi^2$ above results in a isotropic ODF, $w_{\text{iso}} = 1/(8\pi^2)$ (Bunge, 1982; Roe, 1965).

Among the different alternatives, we adopt the following convention to specify rotations through Euler's angles: one begins with the principal material coordinate system x_i' ($i = 1, 2, 3$) fixed to the crystal and with the axes being parallel to those of the global coordinate system x_i ($i = 1, 2, 3$); then x_i' ($i = 1, 2, 3$) is first rotated about the x_3'-axis through the angle ψ; the second rotation is about the x_2'-axis (in its new orientation) through θ and, finally, the third rotation is again about the x_3'-axis (in its new orientation) through the angle ϕ. All positive rotations are in counterclockwise direction.

The piezoelectric components of $\mathbf{e}'$ fixed to a crystal can be expressed in the global coordinate system x_i ($i = 1, 2, 3$) according to the transformation law for third-order tensors

$$e_{ijk}(\xi, \psi, \phi) = \Omega_{im}\Omega_{jn}\Omega_{ko}e'_{mno} = T_{imjnko}e'_{mno}, \tag{4}$$

where $\boldsymbol{\Omega}$ –the matrix representation of the orientation g in the Euler's space– is the orthogonal transformation matrix ($SO(3)$) given by

$$\boldsymbol{\Omega} = \begin{pmatrix} \cos(\theta)\cos(\psi)\cos(\phi) - \sin(\psi)\sin(\phi) & -\cos(\theta)\cos(\psi)\sin(\phi) - \sin(\psi)\cos(\phi) & \sin(\theta)\cos(\psi) \\ \cos(\theta)\sin(\psi)\cos(\phi) + \cos(\psi)\sin(\phi) & \cos(\psi)\cos(\phi) - \cos(\theta)\sin(\psi)\sin(\phi) & \sin(\theta)\sin(\psi) \\ -\sin(\theta)\cos(\phi) & \sin(\theta)\sin(\phi) & \cos(\theta) \end{pmatrix}. \tag{5}$$

The sixth-order matrix T_{imjnko} condenses the triple tensor product $\Omega_{im}\Omega_{jn}\Omega_{ko}$; it possesses major symmetries only (minor symmetries are not present because $\boldsymbol{\Omega}$ is nonsymmetric) given by the permutations of the disjoint cycles of indices

$$\text{Cycles}[(3\,5)(4\,6)],\ \text{Cycles}[(1\,3)(2\,4)],\ \text{Cycles}[(1\,3\,5)(2\,4\,6)]. \tag{6}$$

These symmetries allow a considerable reduction in the number of components of T_{imjnko} to be computed. Thus, of the 729 components of T_{imjnko} only 249 are different.

Finally, the averaging of equation (4) results in

$$\langle e_{ijk}(\xi, \psi, \phi) \rangle = \langle T_{imjnko}e'_{mno} \rangle = \langle T_{imjnko} \rangle e'_{mno}, \tag{7}$$

which shows that the estimation of the effective piezoelectric tensor of the polycrystalline aggregate reduces to finding the $\langle T_{imjnko} \rangle$ for the corresponding ODF.

In what follows, the prime symbol will be dropped from the piezoelectric constants in the crystal coordinate system in order to allow a cleaner notation.

3. Averaging in terms of generalized spherical harmonic series expansions

Following Gel'fand et al. (1963), generalized spherical harmonics form a complete orthogonal basis for the Hilbert space $L^2(SO(3))$, which is the set of all square integrable real-valued functions on $SO(3)$ with inner product defined by

$$(H_1, H_2) = \oint H_1(g)H_2^*(g)\mathrm{d}g, \quad H_1, H_2 \in L^2(SO(3)), \tag{8}$$

where $*$ denotes the complex conjugate. Thus, a general real function $H \in L^2(SO(3))$ can be expanded in series of generalized spherical harmonics. This is a useful approach to evaluate the average of a general real function $\langle H \rangle$. To do this, we expand both the ODF $w(\xi, \psi, \phi)$ and $H(\xi, \psi, \phi)$ into generalized spherical harmonics series (Roe, 1965) as follows:

$$w(\xi, \psi, \phi) = \sum_{l=0}^{\infty} \sum_{m=-l}^{l} \sum_{n=-l}^{l} W_{lmn} Z_{lmn}(\xi) e^{-im\psi} e^{-in\phi}, \tag{9}$$

and

$$H(\xi, \psi, \phi) = \sum_{l=0}^{\infty} \sum_{m=-l}^{l} \sum_{n=-l}^{l} H_{lmn} Z_{lmn}(\xi) e^{-im\psi} e^{-in\phi}, \tag{10}$$

where $\mathrm{i} = \sqrt{-1}$ and $Z_{lmn}(\xi)$ is a generalization of the Legendre associated function P_l^{mn} that can be expressed as

$$Z_{lmn}(\xi) = \mathrm{i}^{n-m} \sqrt{\frac{2l+1}{2}} P_l^{mn}(\xi), \tag{11}$$

being

$$\begin{aligned} P_l^{mn}(\xi) = & \frac{(-1)^{l-m} \mathrm{i}^{n-m}}{2^l (l-m)!} \left[\frac{(l-m)!(l+n)!}{(l+m)!(l-n)!} \right]^{\frac{1}{2}} \\ & \times \frac{(1-\xi)^{\frac{-(n-m)}{2}}}{(1+\xi)^{\frac{(n+m)}{2}}} \frac{d^{l-n}}{d\xi^{l-n}} \left[(1-\xi)^{l-m} (1+\xi)^{l+m} \right] \end{aligned}. \tag{12}$$

The associated Legendre function P_l^{mn} can be either real or purely imaginary, according to whether $m + n$ is even or odd, respectively. Consequently, $Z_{lmn}(\xi)$ is always real-valued.

The coefficients of the expansions in (9) and (10) are (Bunge, 1982; Kocks et al., 2005)

$$W_{lmn} = \frac{1}{4\pi^2} \int_0^{2\pi} \int_0^{2\pi} \int_{-1}^{+1} w(\xi, \psi, \phi) Z_{lmn}(\xi) e^{im\psi} e^{in\phi} d\xi d\psi d\phi, \tag{13}$$

the so-called texture coefficients, and

$$H_{lmn} = \frac{1}{4\pi^2} \int_0^{2\pi} \int_0^{2\pi} \int_{-1}^{+1} H(\xi, \psi, \phi) Z_{lmn}(\xi) e^{im\psi} e^{in\phi} d\xi d\psi d\phi. \tag{14}$$

Note that all information about the ODF is contained in the texture coefficients, which are complex quantities satisfying

$$W_{lmn} = (-1)^{m+n} W_{l\bar{m}\bar{n}}^*, \tag{15}$$

due to the symmetry properties of $Z_{lmn}(\xi)$ (Roe, 1965). In equation (15), $\bar{m} = -m$. From the normalization condition (2), it can be shown that

$$W_{000} = \frac{1}{4\sqrt{2}\pi^2}. \tag{16}$$

In practice, the normalization of $w(\xi, \psi, \phi)$ is preferred by ensuring (16) instead of (2).

Expansion coefficients H_{lmn} are complex and typically involve integration of simple trigonometric functions (H contains products of direction cosines) and the generalized spherical harmonics. Their analytical expressions can be found once H is specified.

Finally, the expansion for the average of a general real function $\langle H \rangle$, is (Bunge, 1982; Kocks et al., 2005)

$$\langle H \rangle = 4\pi^2 \sum_{l=0}^{R} \sum_{m=-l}^{l} \sum_{n=-l}^{l} H_{lmn} W_{lmn}, \tag{17}$$

where, from the truncation theorem by Ferrari and Johnson (1988), $R = 3$, the tensor rank of e_{ijk}. In fact, all coefficients H_{lmn} are zero for $l > 3$.

It is worth to note that, unlike the works by Li (2000); Krishnaswamy et al. (2019a); Li et al. (1999), the present analysis does not imposed any restriction on W_{lmn}. In the next, we will use (17) to obtain the expressions for the average rotation tensor in (7), which, in turn, will be used to compute the effective piezolectric tensor.

4. Effective piezoelectric tensors for all crystal symmetries

Note first that each of the components T_{imjnko} are real functions $T_{imjnko} : SO(3) \rightarrow \mathbb{R}$, similar to function H. Then, derivation of the expressions for the average rotation matrix in (7) can be performed via expression (17). This methodology involves the computation of the coefficients H_{lmn} for each of thse 249 different components of T_{imjnko} according to (14). This was done analytically using Mathematica (2020). Due to space limitations, the full expressions are reported in `Supplementary Material 1`. All 249 components are necessary in order to consider a general case with any symmetry.

Two sources of symmetry are considered when computing the average piezoelectric tensor (7): the ones due to the crystallite structures and the others due to the ODF. No symmetry restrictions are imposed on the ODF –and hence to the texture coefficients in (17)– in this work. In respect to the crystallite symmetries, all the non-centrosymmetrical classes (Nye, 1985) are considered. The expressions of (7) for each of the 21 classes are presented in `Supplementary Material 2`. The $\langle e_{ijk} \rangle$ in `Supplementary Material 2` are functions of the texture coefficients W_{lmn}, which are necessary to specify for each case of analysis according to the adopted ODF. The property (15) has been used to present the expressions of $\langle e_{ijk} \rangle$ in real form. Note that from the 21 non-centrosymmetrical classes only 20 are piezoelectric. Thus, the cubic class 432 results in all components of $\langle e_{ijk} \rangle$ identically zero, no matter what the W_{lmn} are. Some of the piezoelectric classes share the matrix structure reducing the amount of expressions as it can be observed in `Supplementary Material 2`.

Two supplementary materials provide all the details of the main contribution of this work. The next section analyzes the tetragonal *4mm* class in detail.

5. Study problem: Tetragonal class 4mm

The theory introduced above is applied for the analysis of polycrystalline aggregate of $BaTiO_3$ in order to verify and illustrate the derived results. Barium titanate is both a lead-free material (Saito et al., 2004) and environmentally friendly in its processing (Ibn-Mohammed et al., 2017). Interesting novel applications (Wang et al. (2018) among others) have been proposed while $BaTiO_3$-based composites can be fabricated in a scalable manner using emerging additive manufacturing methods (Kim et al., 2017, 2019; Phatharapeetranun et al., 2017). Li (2000), among others (see for example (Li et al., 1999; Ruglovsky et al., 2006)), has studied the average piezoelectric properties of $BaTiO_3$ polycrystalline aggregates.

The $BaTiO_3$ crystal belongs to the point group class *4mm*, with their piezoelectric constants listed in Table 1 (Li, 2000). Thus, the expressions for the average components $\langle e_{ijm} \rangle$ for the tetragonal symmetry are retrieved from `Supplementary Material 2` and summarized below:

$$\langle e_{111} \rangle = -\frac{4}{105}\pi^2 \left(\sqrt{14}(5e_A - e_B)\Re\left(\sqrt{3}W_{310} - \sqrt{5}W_{330}\right) + 14\sqrt{3}e_B\Re(W_{110}) \right), \tag{18}$$

$$\langle e_{122} \rangle = \frac{4}{315}\pi^2 \left(14\sqrt{3}\Re(W_{110})(2e_A - e_B + 3e_C) + \sqrt{14}(e_B - 5e_A)\Re\left(\sqrt{3}W_{310} + 3\sqrt{5}W_{330}\right) \right), \tag{19}$$

$$\langle e_{133} \rangle = \frac{8\pi^2 \left(7\Re(W_{110})(2e_A - e_B + 3e_C) + 2\sqrt{14}(5e_A - e_B)\Re(W_{310}) \right)}{105\sqrt{3}}, \tag{20}$$

$$\langle e_{123} \rangle = \frac{8\pi^2(5e_A - e_B)\Im(W_{320})}{3\sqrt{105}}, \tag{21}$$

$$\langle e_{113} \rangle = \frac{2}{315}\pi^2 \left(7\sqrt{6}\Re(W_{100})(2(e_A + e_B) + 3e_C) + 2\sqrt{7}(5e_A - e_B)\Re\left(3\sqrt{2}W_{300} - 2\sqrt{15}W_{320}\right) \right), \tag{22}$$

$$\langle e_{112} \rangle = \frac{4}{315}\pi^2 \left(7\sqrt{3}\Im(W_{110})(2(e_A + e_B) + 3e_C) + \sqrt{14}(5e_A - e_B)\Im\left(\sqrt{3}W_{310} - 3\sqrt{5}W_{330}\right) \right), \tag{23}$$

$$\langle e_{211} \rangle = -\frac{4}{315}\pi^2 \left(14\sqrt{3}\Im(W_{110})(2e_A - e_B + 3e_C) + \sqrt{14}(e_B - 5e_A)\Im\left(\sqrt{3}W_{310} - 3\sqrt{5}W_{330}\right) \right), \tag{24}$$

$$\langle e_{222} \rangle = \frac{4}{105}\pi^2 \left(\sqrt{14}(5e_A - e_B)\Im\left(\sqrt{3}W_{310} + \sqrt{5}W_{330}\right) + 14\sqrt{3}e_B\Im(W_{110}) \right), \tag{25}$$

$$\langle e_{233} \rangle = \frac{8}{105\sqrt{3}} \pi^2 \left(7\Im(W_{110})(-2e_A + e_B - 3e_C) + \right.$$
$$\left. 2\sqrt{14}(e_B - 5e_A)\Im(W_{310}) \right), \tag{26}$$

$$\langle e_{223} \rangle = \frac{2}{315} \pi^2 \left(7\sqrt{6}\Re(W_{100})(2(e_A + e_B) + 3e_C) + \right.$$
$$\left. 2\sqrt{7}(5e_A - e_B)\Re\left(3\sqrt{2}W_{300} + 2\sqrt{15}W_{320} \right) \right), \tag{27}$$

$$\langle e_{213} \rangle = \frac{8\pi^2(5e_A - e_B)\Im(W_{320})}{3\sqrt{105}}, \tag{28}$$

$$\langle e_{212} \rangle = -\frac{4}{315} \pi^2 \left(7\sqrt{3}\Re(W_{110})(2(e_A + e_B) + 3e_C) + \right.$$
$$\left. \sqrt{14}(5e_A - e_B)\Re\left(\sqrt{3}W_{310} + 3\sqrt{5}W_{330} \right) \right), \tag{29}$$

$$\langle e_{311} \rangle = -\frac{4}{315} \pi^2 \left(7\sqrt{6}\Re(W_{100})(2e_A - e_B + 3e_C) + \right.$$
$$\left. \sqrt{7}(e_B - 5e_A)\Re\left(3\sqrt{2}W_{300} - 2\sqrt{15}W_{320} \right) \right), \tag{30}$$

$$\langle e_{322} \rangle = -\frac{4}{315} \pi^2 \left(7\sqrt{6}\Re(W_{100})(2e_A - e_B + 3e_C) + \right.$$
$$\left. \sqrt{7}(e_B - 5e_A)\Re\left(3\sqrt{2}W_{300} + 2\sqrt{15}W_{320} \right) \right), \tag{31}$$

$$\langle e_{333} \rangle = \frac{4}{105} \left(2\sqrt{14}\pi^2(e_B - 5e_A)\Re(W_{300}) + 7\sqrt{6}\pi^2 e_B \Re(W_{100}) \right), \tag{32}$$

$$\langle e_{323} \rangle = \frac{4}{105\sqrt{3}} \pi^2 \left(7\Im(W_{110})(2(e_A + e_B) + 3e_C) + \right.$$
$$\left. 4\sqrt{14}(e_B - 5e_A)\Im(W_{310}) \right), \tag{33}$$

$$\langle e_{313} \rangle = -\frac{4}{105\sqrt{3}} \pi^2 \left(7\Re(W_{110})(2(e_A + e_B) + 3e_C) + \right.$$
$$\left. 4\sqrt{14}(e_B - 5e_A)\Re(W_{310}) \right), \tag{34}$$

and

$$\langle e_{312} \rangle = \frac{8\pi^2(5e_A - e_B)\Im(W_{320})}{3\sqrt{105}}, \tag{35}$$

where $e_A = 2e_{113} + e_{311}$, $e_B = 4e_{113} + 2e_{311} + 3e_{333}$ and $e_C = 2e_{113} - 4e_{311}$. Note that this set of analytical expressions reduce to those presented by Li (2000) when ODF is such that texture coefficient W_{320} vanishes. However, expressions (18) - (35) are more general as shown below.

To verify these results, we first consider the ODF

$$w_\delta(\xi, \psi, \phi) = \delta(\xi - 1), \tag{36}$$

where $\delta(\xi - 1)$ is the Dirac delta function at $\xi = 1$. This ODF describes an aggregate with all the crystallites oriented with $\theta = 0$ and random values for ψ and ϕ, which

Table 1. Piezoelectric constants of tetragonal BaTiO$_3$ single crystal (Cm^{-2}) (Li, 2000).

$e_{113} = e_{223}$	$e_{311} = e_{322}$	e_{333}
21.3	-2.69	3.65

means that the piezoelectric is a perfectly oriented polycrystal in the x_3' orientation. By substituing (36) into equation (13), we obtain the following non-vanishing texture coefficients:

$$W_{100}^{\delta} = \frac{\sqrt{\frac{3}{2}}}{4\pi^2}, \tag{37}$$

and

$$W_{300}^{\delta} = \frac{\sqrt{\frac{7}{2}}}{4\pi^2}. \tag{38}$$

Due to the six-fold axis symmetry of the tetragonal crystal with the x_3'-axis, the BaTiO$_3$ single crystal properties should be recovered from the effective properties of the polycrystal. This was successfully verified by substituting the texture coefficients (37) and (38) into (18)-(35). The same verification was performed for all the formulas for the different crystal symmetries in `Supplementary Material 2`. In this case, when the ODF is given by

$$w_{\delta}(\xi, \psi, \phi) = \delta(\xi - 1)\delta(\psi)\delta(\phi), \tag{39}$$

the non-zero texture coefficients used for these verifications are:

$$W_{1\bar{1}\bar{1}}^{\delta} = W_{100}^{\delta} = W_{111}^{\delta} = \frac{\sqrt{\frac{3}{2}}}{4\pi^2}, \tag{40}$$

$$W_{2\bar{2}\bar{2}}^{\delta} = W_{2\bar{1}\bar{1}}^{\delta} = W_{200}^{\delta} = W_{211}^{\delta} = W_{222}^{\delta} = \frac{\sqrt{\frac{5}{2}}}{4\pi^2}, \tag{41}$$

and

$$W_{3\bar{3}\bar{3}}^{\delta} = W_{3\bar{2}\bar{2}}^{\delta} = W_{3\bar{1}\bar{1}}^{\delta} = W_{300}^{\delta} = W_{311}^{\delta} = W_{322}^{\delta} = W_{333}^{\delta} = \frac{\sqrt{\frac{7}{2}}}{4\pi^2}. \tag{42}$$

This paper used both generalized spherical harmonics ODF and Gaussian ODF for model derivation, but did not discuss the relationship between them. This may cause confusion to readers. These two types of ODF can be unified or connected in general, as discussed in the Reference [1] below.

Next, two Gaussian ODFs are considered. Gaussian ODFs allow for the analytical integration of the texture coefficients and for the comparison with results published in the literature. These analytical Gaussian ODFs are not the series expansion

representation ODFs given by equation (9) so this should not cause confusion. These two ODFs are clearly related as discussed by Sha (2018).

First, we consider the simple (fiber texture) Gaussian ODF

$$w_A(\theta \,|\, \mu_\theta, \sigma_\theta) = \frac{\exp\left(-\frac{(\theta-\mu_\theta)^2}{2\sigma_\theta^2}\right)}{\sqrt{2\pi}\sigma_\theta}, \tag{43}$$

where μ_θ is the mean of the Euler's angle θ, and σ_θ is its standard deviation. The orientations due to angles ψ and ϕ are assumed to be randomly distributed. The ODF w_A is used to compute the texture coefficients through equation (13). This results in only two non-zero texture coefficients, W_{100}^A and W_{300}^A, that are reported in `Supplementary Material 3`. Note that these expressions reduce to those presented by the authors in Ref. Krishnaswamy et al. (2019a) for $\mu_\theta = 0$. The texture coefficients in `Supplementary Material 3` together with (18-35) provide the fully analytic expressions for the effective piezoelectric tensor of a BaTiO$_3$ (or any *4mm* class crystal) aggregate with the ODF in equation (43). The effective piezoelectric tensor is obtained after replacing W_{100}^A and W_{300}^A in equations (18-35). Figure 1 shows the components of the three non-zero components of the effective piezoelectric stress tensor, $\langle e_{113} \rangle$, $\langle e_{311} \rangle$ and $\langle e_{333} \rangle$, as functions of the Gaussian distribution parameter σ_θ. The results for $\mu_\theta = 0$ –the continuous lines in the plot– are in perfect agreement with those by Li (2000). Discontinuous lines show the results for $\mu_\theta = \pi/12$ and $\pi/6$.

The asymptotic behaviors of $\langle e_{ijk} \rangle$ are clear from Figure 1. For $\sigma_\theta \to \infty$, W_{100}^A and W_{300}^A tend both to zero, as well as all the components of $\langle e_{ijk} \rangle$; this behavior reflects the fact that the aggregate has null effective piezoelectric properties for a fully random distribution of the crystals. For the other extreme case, $\sigma_\theta \to 0$, the Gaussian distribution w_A tends to the Dirac delta function w_δ and hence all crystals have identical orientation in x_3-axis, so the single crystal properties are recovered for the aggregate behaviour, as shown in the example above. In accordance with this, the effective values for $\mu_\theta = 0$ in Figure 1 for $\sigma_\theta \to 0$ converge toward the crystal values in Table 5. The same behavior is verified for $\mu_\theta = \pi/12$ and $\pi/6$, however, for these cases, it is necessary to consider that the global coordinate system ($x_i, i = 1 \ldots 3$) does not coincide with that of the crystals; consequently the limit values for the two cases with $\mu_\theta \neq 0$ are those of Table 5 but rotated by the corresponding μ_θ.

Figure 1 also allows observing the marked amplification effects on $\langle e_{311} \rangle$ and $\langle e_{333} \rangle$ for $\mu_\theta = 0$ at $\sigma_\theta \simeq 0.6$, with absolute peak values greater than those of the single crystal. This effect was also noted by Li (2000). In addition, we can see here that the positions of the maximums shift towards lower dispersion values when the mean orientation direction moves away from x_3, i.e. when $\mu_\theta \neq 0$. To better illustrate this, the 3D plot in Figure 2 shows the combined effects of σ_θ and μ_θ on $\langle e_{333} \rangle$. It can be observed that the overall maximum $\langle e_{333} \rangle_{\max} = 16.116$ C/m^2 is for $\mu_\theta = 0.92$ rad in the limit case $\sigma_\theta \to 0$, that is, the maximum coupling effect that can be achieved by rotating a single crystal.

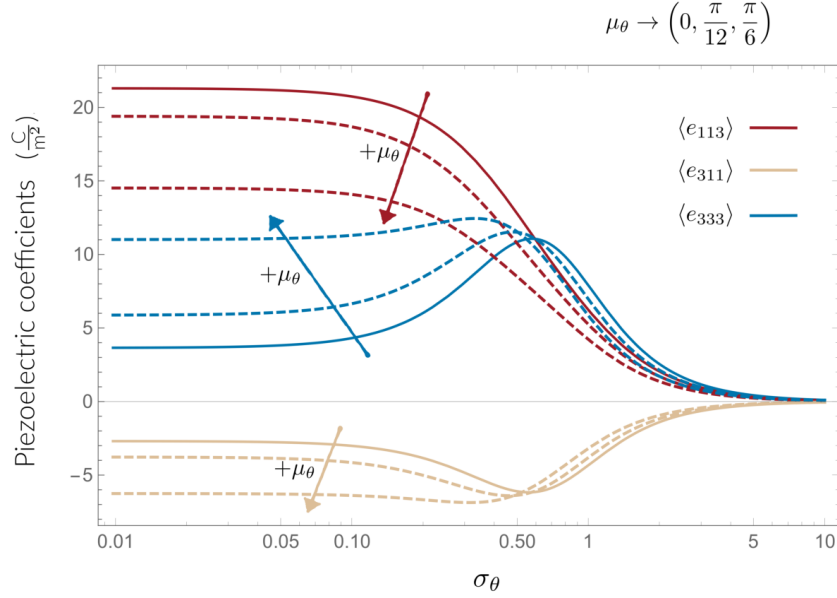The second case of analysis is an aggregate with biaxial Gaussian distributions for

$$\mu_\theta \to \left(0, \frac{\pi}{12}, \frac{\pi}{6}\right)$$

Figure 1. Effective piezoelectric moduli of polycrystal BaTiO$_3$ as a function of the Gaussian distribution parameter σ_θ. Continuous lines represent the constants for a mean value $\mu_\theta = 0$. Discontinuous lines correspond to mean values of $\mu_\theta = \pi/12$ and $\pi/6$.
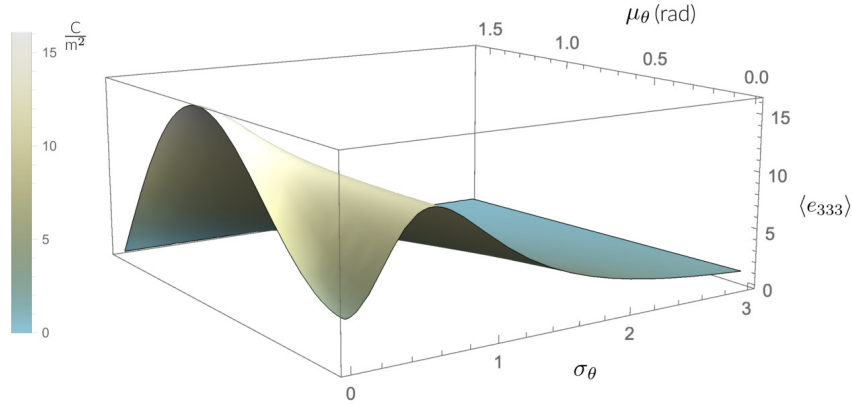

Figure 2. Effective piezoelectric constant $\langle e_{333} \rangle$ of polycrystal BaTiO$_3$ as a function of the mean value μ_θ of the Euler's angle θ, and the Gaussian distribution parameter σ_θ.

ψ and θ (Ruglovsky et al., 2006) given by

$$w_B(\theta \,|\, \mu_\theta, \sigma_\theta; \psi \,|\, \mu_\psi, \sigma_\psi) = \frac{\exp\left(-\frac{(\theta - \mu_\theta)^2}{2\sigma_\theta^2} - \frac{(\psi - \mu_\psi)^2}{2\sigma_\psi^2}\right)}{2\pi\sigma_\theta\sigma_\psi}, \tag{44}$$

and a random distribution for ϕ (in fact, due to the tetragonal symmetry of the BaTiO$_3$, the behaviour of the aggregate is independent of ϕ).

The evaluation of equation (13) for w_B results in 6 texture coefficients, these are: W_{100}^B, W_{110}^B, W_{300}^B, W_{310}^B, W_{320}^B and W_{330}^B. The analytic expressions of the coefficients are given in `Supplemtary Material 3`. Coefficients W_{110}^B, W_{310}^B, W_{320}^B and W_{330}^B are complex-valued, meanwhile W_{100}^B and W_{300}^B are real. Moreover, W_{100}^B and W_{300}^B are equal to W_{100}^A and W_{300}^A (the texture coefficients of the first case of analysis) and so, independent of ψ and σ_ψ.

The behavior of the texture coefficients strongly depends on the parameter values. As examples, Figures 3 and 4 show the diversity of behaviors of the real and imaginary parts of the texture coefficients as functions of σ_θ for the arbitrary set of parameters $\mu_\theta = 0$, $\mu_\psi = \pi/3$ and $\sigma_\psi = 1$; Figures 5 and 6 do so as function of σ_ψ for $\mu_\theta = 0$, $\mu_\psi = \pi/3$ and $\sigma_\theta = 0.6$. It is observed that some of the texture coefficients vanish for standard deviations tending to infinity or tending to zero, while others do not.

It is interesting to analyze the limiting case $\sigma_\theta \to 0$ for Figures 3 and 4. Note that both the real and imaginary parts of all the complex coefficients vanish, and the real texture coefficients take the values $W_{100}^B \equiv W_{100}^\delta$ and $W_{300}^B \equiv W_{300}^\delta$, (see equations (37) and (38)). These results can be verified by taking the limits of the expressions for W_{100}^B and W_{300}^B in `Supplementary Material 3`. For this limit, the x_3-axis of the polycrystal coincides with the global x_3-axis and the x_1'-axis is rotated $\mu_\psi = \pi/3$ with respect to the x_1-axis. Due to the tetragonal symmetry of the $BaTiO_3$, the piezoelectric tensor is invariant under rotations about x_3'-axis, and as a consequence, the effective properties of the polycrystal are the same as the crystal. For the other limiting case, $\sigma_\theta \to \infty$, Figures 3 and 4 show that only a few texture coefficients vanish and the resulting effective piezoelectric tensor is transversely isotropic with x_2 as the symmetry axis.

Figures 5 and 6 show that all texture coefficients converge to finite values for the limiting case $\sigma_\psi \to 0$, which results in a fully populated matrix for the effective piezoelectric behaviour. Conversely, the real and imaginary parts of all complex coefficients vanish for $\sigma_\psi \to \infty$, that is, when Euler's angle ψ is randomly distributed. In this situation, only the terms that contain the coefficients W_{100}^B and W_{300}^B will remain in equations (18-35) to obtain expressions for $\langle e_{223} \rangle$, $\langle e_{311} \rangle$ and $\langle e_{333} \rangle$ that match those of the previous case of analysis. It can also be verified that in the case where $\sigma_\psi \to \infty$ and $\sigma_\theta \to \infty$ simultaneously, regardless of the values of μ_ψ and μ_θ, all the texture coefficients vanish and so an isotropic material with no piezoelectric properties is obtained.

Figure 7 shows all the 18 components of $\langle e_{ijk} \rangle$ of the polycrystal as functions of σ_θ for $\mu_\theta = 0$, $\mu_\psi = \pi/3$ and $\sigma_\psi = 1$ (the same parameters for the texture coefficients in Figures 5 and 6). It is clear that all components can be different from zero for a general case. Figure 8 shows, in particular, the behavior of $\langle e_{112} \rangle$ as a function of the mean value for the first Euler's angle, μ_ψ, and its dispersion, σ_ψ, when $\mu_\theta = 0$ and $\sigma_\theta = 0.6$. The minimum value $\langle e_{112} \rangle_{\min} = -12.854$ C/m^2 was found for $\mu_\psi = \pi/2$ rad and zero dispersion ($\sigma_\psi = 0$).

In virtue of the symmetry $e_{ijk} = e_{ikj}$ ($i, j, k = 1 \ldots 3$), the usual two-index reduction mapping $e_{ijk} \mapsto e_{i\alpha}$ ($\alpha = 1 \ldots 6$) is used to represent the results in matrix form, according
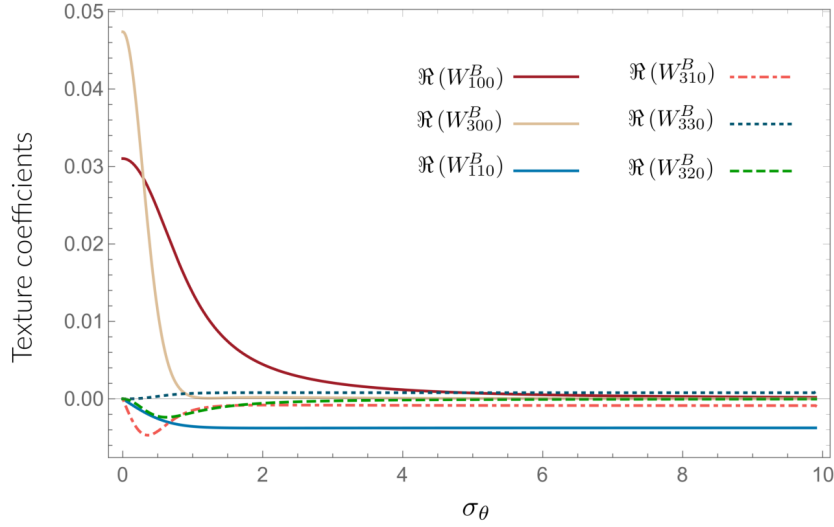
Figure 3. Real parts of the texture coefficients W_{lmn} as functions of Gaussian distribution parameter σ_θ when the mean values are $\mu_\theta = 0$ and $\mu_\psi = \pi/3$, and $\sigma_\psi = 1$.
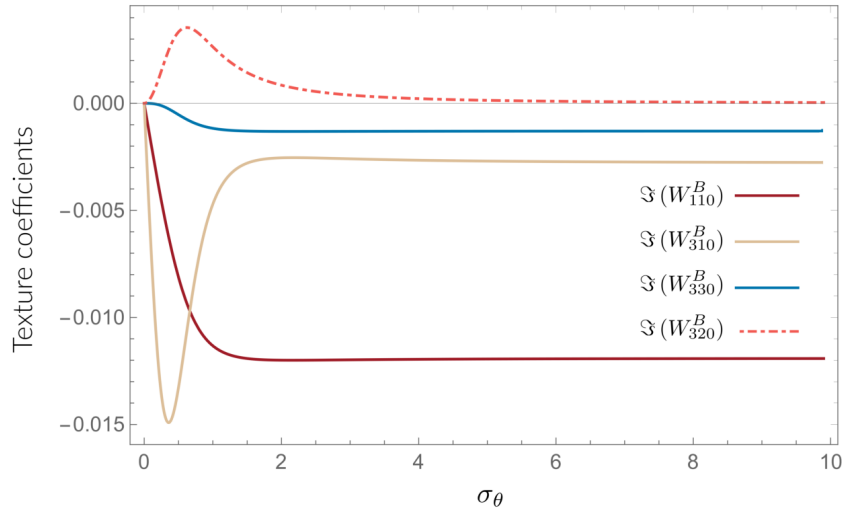

Figure 4. Imaginary parts of the texture coefficients W_{lmn} as functions of Gaussian distribution parameter σ_θ when the mean values are $\mu_\theta = 0$ and $\mu_\psi = \pi/3$, and $\sigma_\psi = 1$.

to the next set of index rules $km \mapsto \alpha$: $11 \mapsto 1, 22 \mapsto 2, 33 \mapsto 3, 23 \mapsto 4, 13 \mapsto 5, 12 \mapsto 6$. Thus, Table 2 compares the matrix structures of the effective piezoelectric coupling tensors resulting from the two Gaussian ODFs (see Figures 1 and 7). It can be observed that the simple Gaussian ODF for the Euler's angle θ (the line labelled w_A) results always in a polycrystal with an effective piezoelectric tensor with the same point-group class $4mm$ symmetry of the single crystal. On the other hand, the double Gaussian ODF for
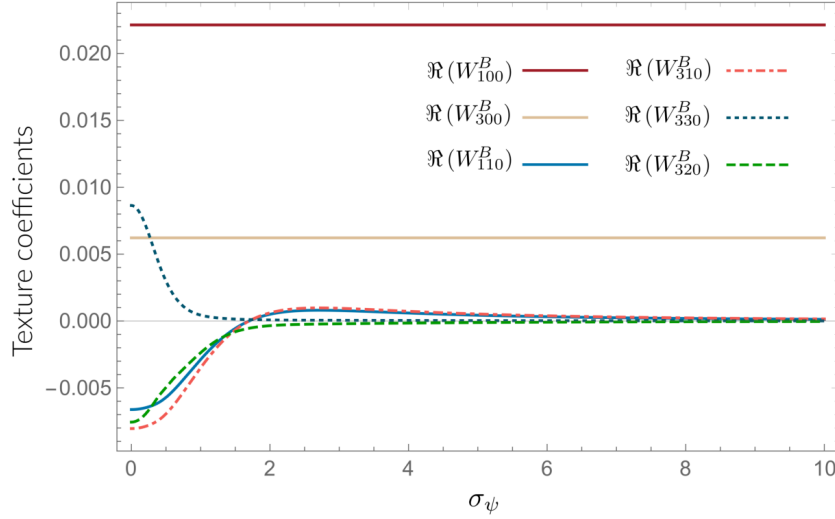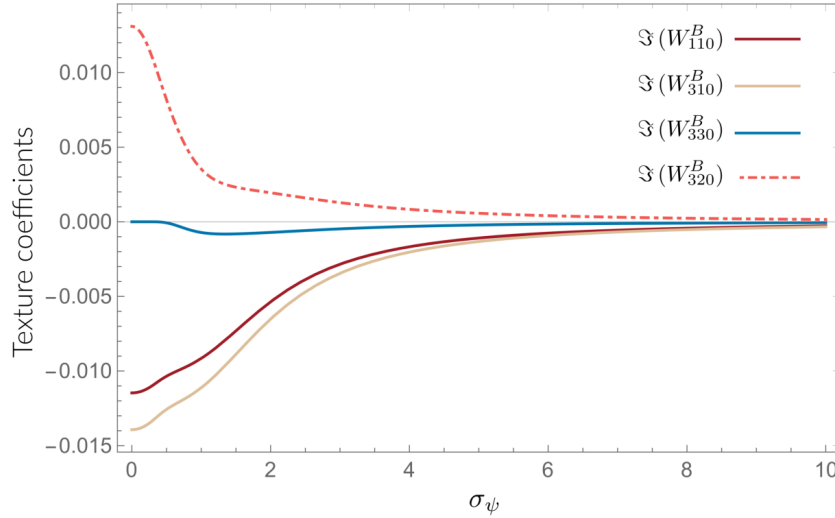
Figure 5. Real parts of the texture coefficients W_{lmn} as functions of Gaussian distribution parameter σ_ψ when the mean values are $\mu_\theta = 0$ and $\mu_\psi = \pi/3$, and $\sigma_\theta = 0.6$.

Figure 6. Imaginary parts of the texture coefficients W_{lmn} as functions of Gaussian distribution parameter σ_ψ when the mean values are $\mu_\theta = 0$ and $\mu_\psi = \pi/3$, and $\sigma_\theta = 0.6$.

the Euler's angles θ and ψ (the line labelled w_B) can produce a fully-populated effective piezoelectric tensor.

Also it can be noted that $\langle e_{123} \rangle$, $\langle e_{213} \rangle$ and $\langle e_{312} \rangle$ are equal, thus resulting –for the w_B ODF– in a matrix structure as shown in Table 2.
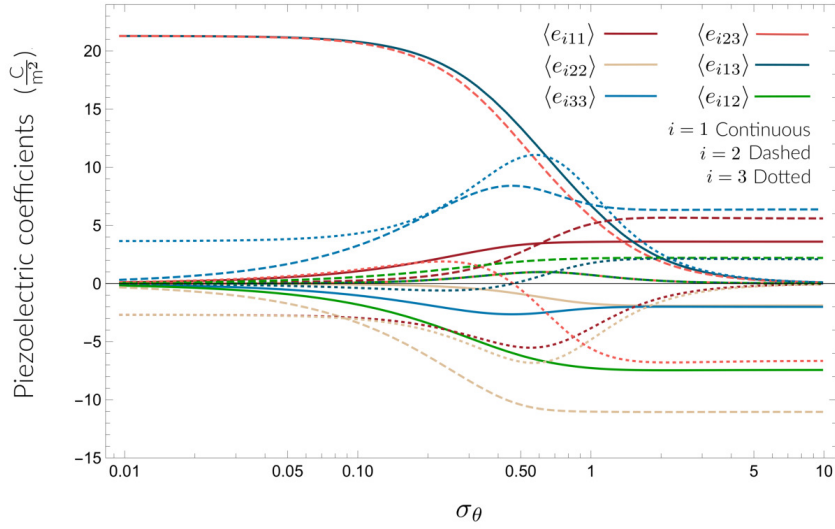
Figure 7. Effective piezoelectric moduli of polycrystal $BaTiO_3$ as a function of the Gaussian distribution parameter σ_θ for $\mu_\theta = 0$, $\mu_\psi = \pi/3$ and $\sigma_\psi = 1$.
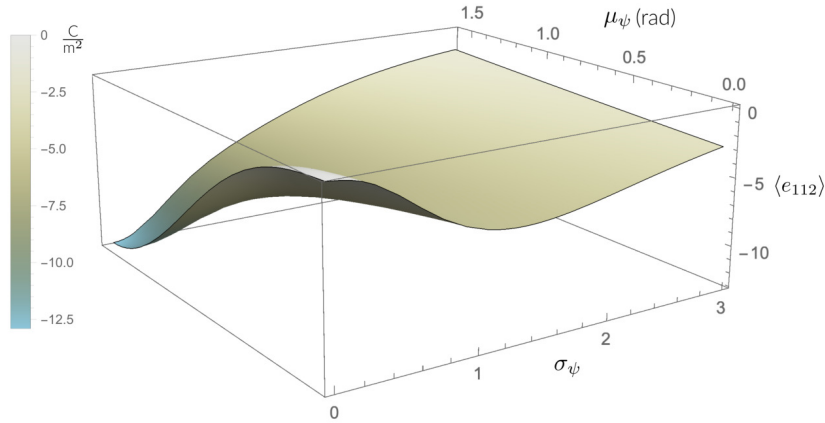

Figure 8. Effective piezoelectric constant $\langle e_{112} \rangle$ of the $BaTiO_3$ polycrystal as a function of μ_ψ and σ_ψ for $\mu_\theta = 0$ and $\sigma_\theta = 0.6$.

Table 2. Matrix structures of the effective piezoelectric coupling tensors resulting from the two Gaussian ODFs.

ODF	Crystal matrix structure	Polycrystal matrix structure
w_A	$\begin{pmatrix} 0 & 0 & 0 & 0 & e_{223} & 0 \\ 0 & 0 & 0 & e_{223} & 0 & 0 \\ e_{311} & e_{311} & e_{333} & 0 & 0 & 0 \end{pmatrix}$	$\begin{pmatrix} 0 & 0 & 0 & 0 & \langle e_{223} \rangle & 0 \\ 0 & 0 & 0 & \langle e_{223} \rangle & 0 & 0 \\ \langle e_{311} \rangle & \langle e_{311} \rangle & \langle e_{333} \rangle & 0 & 0 & 0 \end{pmatrix}$
w_B	$\begin{pmatrix} 0 & 0 & 0 & 0 & e_{223} & 0 \\ 0 & 0 & 0 & e_{223} & 0 & 0 \\ e_{311} & e_{311} & e_{333} & 0 & 0 & 0 \end{pmatrix}$	$\begin{pmatrix} \langle e_{111} \rangle & \langle e_{122} \rangle & \langle e_{133} \rangle & \langle e_{123} \rangle & \langle e_{113} \rangle & \langle e_{112} \rangle \\ \langle e_{211} \rangle & \langle e_{222} \rangle & \langle e_{233} \rangle & \langle e_{223} \rangle & \langle e_{123} \rangle & \langle e_{212} \rangle \\ \langle e_{311} \rangle & \langle e_{322} \rangle & \langle e_{333} \rangle & \langle e_{323} \rangle & \langle e_{313} \rangle & \langle e_{123} \rangle \end{pmatrix}$

6. Conclusions

This work provides general analytical expressions for volume averages of piezoelectric properties of polycrystalline aggregates. The expressions are derived from orientational averages of third-order piezoelectric tensors that are weighted by orientational distribution functions that account for texture. The expressions are derived by using spherical harmonic series expansions.

Improvements of this work with respect to the previous works in the literature are twofold: all crystal symmetries are considered and no symmetry restrictions are imposed to texture. Thus, this work provides the analytical formulas to compute the average piezoelectric tensor of polycrystalline aggregates formed by crystals of all the 21 non-centrosymmetrical classes. These expressions are open to be specialized for any texture, which is specified in terms of Euler´s angles (ψ, θ, ϕ).

The versatility of the introduced expressions is demonstrated for BaTiO$_3$ polycrystals with uniaxial texture given by a single Gaussian dispersion for θ, and with biaxial texture given by a double Gaussian dispersion for θ and ψ. The results for the first case, which consisted in a Gaussian distribution centered around $\theta = 0$, showed to be in perfect agreement with results published in the literature. This case has the particularity that all the texture coefficients and all the expressions of the average piezoelectric properties are real. On the other hand, no previous study was found to verify the results for the simple Gaussian distributions with mean value $\theta \neq 0$ and for the case with biaxial textures. The biaxial texture leads to complex-valued texture coefficients and complex formulations for the averaged piezoelectric properties. Results for the BaTiO$_3$ polycrystal with biaxial texture have been discussed in detail and analyzed for a set of limiting cases. In all cases, the results showed to be consistent.

The main contribution of this work is the set of analytical expressions that simplifies obtaining closed-form formulas to estimate the effective piezoelectric properties of polycrystals with arbitrary symmetries and textures. These expressions are suitable to perform parametric studies like those presented in this work for BaTiO$_3$ polycrystals, and –provided the textures characterized by smooth ODFs– to implement efficient analytical optimization methods to find configurations at the microstructural level in order to maximize piezoelectricity.

It is straightforward to adapt the expression herein derived for the piezoelectric stress tensor **e** to other piezoelectric properties, such as **d**, **g**, **h** (see IEEE Standard on Piezoelectricity (1988)) or the piezomagnetic moduli.

Author's contributions

JLB: Investigation, Software, Validation, FCB: Conceptualization, Formal Analysis, Methodology, Visualization, Project Administration, Writing - Original draft preparation, Review & Editing, APC: Supervision, Resources, Writing - Original draft preparation, Review & Editing, RM: Writing – Review & Editing, LRT: Project

Administration, Writing - Review, AS: Writing - Review

Acknowledgments

Data Availability

The data that supports the findings of this study are available within the article [and its supplementary material].

References

Bunge, H. 1982. Texture analysis in Materials Science. Butterworths, London.

Ferrari, M., Johnson, G.C. The equilibrium properties of a 6 mm polycrystal exhibiting transverse isotropy. *Journal of Applied Physics* vol. 63, 4460 - 4468, 1988

Gel'fand, I. M., Minlos, R. A., Cummins, G. 1963. Representations of the Rotation and Lorentz Groups and Their Applications. Macmillan

IEEE Standard on Piezoelectricity, in ANSI/IEEE Std 176-1987 , 1988. (DOI: 10.1109/IEEESTD.1988.79638)

Jayachandran, K.P., Guedes, J.M., Rodrigues, H.C.. Ferroelectric materials for piezoelectric actuators by optimal design. *Acta Materialia*, 59(10), 3770–3778, 2011

Kim, H-S., Hyun, T-S., Kim, H-G., Kim, I-D., Yun, T-S., Lee, J-C. Orientation effect on microwave dielectric properties of Si-integrated Ba0.6Sr0.4TiO3 thin films for frequency agile devices. *Appl. Phys. Lett.* 89 0529021–3, 2006

Kim, H., Torres,F., Villagran, D., Stewart, C., Lin, Y., Tseng, T.-L. B. 3D Printing of BaTiO3/PVDF Composites with Electric In Situ Poling for Pressure Sensor Applications. *Macromolecular Materials and Engineering.* 302, (11), 1700229, 2017

Kim, H., Wilburn, B.R., Castro, E., Garcia Rosales, C.A., Chavez, L.A., Tseng, T-L. B., Lin, Y. Multifunctional SENSING using 3D printed CNTs/BaTiO3/PVDF

nanocomposites. *Journal of Composite Materials*, 53(10), 1319–1328, 2019

Kocks, U. F., Tomé, C. N., Wenk, H.-R. 2005. Texture and Anisotropy. Preferred orientations in polycrystals and their effect on materials properties. Cambridge University Press

Krishnaswamy, J.A., Buroni, F.C., García-Sánchez, F., Melnik, R., Rodríguez-Tembleque, R., Sáez, A. Improving the performance of lead-free piezoelectric composites by using polycrystalline inclusions and tuning the dielectric matrix environment. *Smart Materials & Structures*, vol. 28, 075032, 2019

Krishnaswamy, J.A., Buroni, F.C., García-Sánchez, F., Melnik, R., Rodríguez-Tembleque, R., Sáez, A. Lead-free piezocomposites with CNT-modified matrices: Accounting for agglomerations and molecular defects. *Composite Structures*, vol. 224, pp. 111033, 2019

Krishnaswamy, J.A., Buroni, F.C., García-Macías, E., Melnik, R., Rodríguez-Tembleque, R., Sáez, A. Design of lead-free PVDF/CNT/BaTiO3 piezocomposites for sensing and energy harvesting: The role of polycrystallinity, nanoadditives, and anisotropy. *Smart Materials & Structures*, vol. 29, 015021 (13pp), 2020

Krishnaswamy, J.A., Buroni, F.C., García-Macías, E., Melnik, R., Rodríguez-Tembleque, R., Sáez, A. Design of nano-modified PVDF matrices for lead-free piezocomposites: Graphene vs carbon nanotube nano-additions. *Mechanics of Materials* vol. 142, 103275, 2020

Krishnaswamy, J.A., Buroni, F.C., Melnik, R., Rodríguez-Tembleque, R., Sáez, A. Advanced modeling of lead-free piezocomposites: The role of nonlocal and nonlinear effects. *Composite Structures*, vol. 238, pp. 111967, 2020

Ibn-Mohammed, T., Koh, S., Reaney, I., Sinclair, D., Mustapha, K., Acquaye, A., Wang, D. Are lead-free piezoelectrics more environmentally friendly? *MRS Communications*, 7(1), 1-7, 2017

Li, J. Y. The effective electroelastic moduli of textured piezoelectric polycrystalline aggregates *Journal of Mechanics and Physics of Solids*, 48 529–52, 2000

Li, J. Y., Dunn, M. L., Ledbetter, H . Thermoelectroelastic moduli of textured piezoelectric polycrystals: Exact solutions and bounds for film textures. *Journal of Applied Physics* vol. 96, 4626-4634, 1999

Li, J. Y., Dunn, M. L., Variational bounds for the eVective moduli of heterogeneous piezoelectric solids. *Philosophical Magazine A* vol. 81, 903-926, 2001

Li, J.Y., . Rogan, R.C, Ustundag, E. , Bhattacharya, K. Domain switching in polycrystalline ferroelectric ceramics. *Nature Materials* 4 776–81, 2005

Mathematica, Version 12.1. (Champaign IL.) Wolfram Research, Inc.; 2020.

Nye, J. F. 1985. Physical Properties of Crystals. Clarendon Press — Oxford

Phatharapeetranun, N., Ksapabutr, B., Marani, D., Bowen, J.R., Esposito, V. 3D-printed barium titanate/poly-(vinylidene fluoride) nano-hybrids with anisotropic dielectric properties. *Journal of Materials Chemistry C*, 5, 12430–12440, 2017

Roe, R-J. Description of Crystallite Orientation in Polycrystalline Materials. III. General Solution to Pole Figure Inversion. *Journal of Applied Physics* 36, 2024, 1965

Ruglovsky, J.L., Li, J.Y., Bhattacharya, K., Atwater, H.A.. The effect of biaxial texture on the effective electromechanical constants of polycrystalline barium titanate and lead titanate thin films. Acta Materialia 54 3657-3663, 2006

Saito, Y., Takao, H., Tani, T., Nonoyama, T., Takatori, K., Homma, T., Nagaya, T. and Nakamura, M. Lead-free piezoceramics. *Nature* 432, pp.84, 2004

Sha, G. Explicit Backscattering Coefficient for Ultrasonic Wave Propagating in Hexagonal Polycrystals with Fiber Texture. *Journal of Nondestructive Evaluation* 37:51, 2018.

Uchino, K. 2017, Advanced Piezoelectric Materials. Science and Technology. Woodhead Publishing

Wang, D., Du, H., Wang, L., Melnik, R. A phase field approach for the fully coupled thermo-electro-mechanical dynamics of nanoscale ferroelectric actuators. *Smart Materials & Structures*, 27 055012, 2018
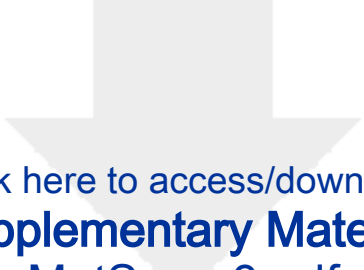
Click here to access/download
Supplementary Material
MatSupp 1.pdf

Click here to access/download
Supplementary Material
MatSupp 2.pdf

Click here to access/download
Supplementary Material
MatSupp 3.pdf